IEEE Access
Multidisciplinary | Rapid Review | Open Access Journal

Received December 16, 2018, accepted December 27, 2018, date of publication January 9, 2019, date of current version January 29, 2019.

Digital Object Identifier 10.1109/ACCESS.2019.2891208

On the Development of a Novel Mixed Embroidered-Woven Slot Antenna for Wireless Applications

LETICIA ALONSO-GONZÁLEZ, (Member, IEEE), SAMUEL VER-HOEYE, (Member, IEEE), MIGUEL FERNÁNDEZ-GARCÍA, CARLOS VÁZQUEZ-ANTUÑA, AND FERNANDO LAS-HERAS ANDRÉS, (Senior Member, IEEE)

Área de Teoría de la Señal y Comunicaciones, Departamento de Ingeniería Eléctrica, Universidad de Oviedo, 33203 Gijón, Spain

Corresponding author: Leticia Alonso-González (alonsoleticia@uniovi.es)

This work was supported in part by the Spanish Agencia Estatal de Investigación (AEI), in part by the Fondo Europeo de Desarrollo Regional (FEDER) under Project TEC2016-80815-P (AEI/FEDER-UE) and Project TEC2015-72110-EXP (AEI) and Grant FPU14/00016, and in part by the Gobierno del Principado de Asturias (PCTI/FEDER-FSE) under Project IDI/2016/000372 and Project IDI/2017/000083.

ABSTRACT A novel mixed embroidered-woven coaxial-fed antenna based on a slotted short-circuited textile integrated waveguide has been designed, manufactured, and experimentally validated for its use in wireless applications. The structure of the antenna and the radiating slot can be manufactured using an industrial loom and a laser prototyping machine, respectively, whereas the conductive vias can be manufactured using a commercial embroidery machine, avoiding subsequent treatments or coating. The manufactured antenna presents a central working frequency of 5 GHz and a 20% bandwidth. Good agreement between simulations and measurements has been achieved. In addition, the performance of the antenna has been simulated and analyzed under bent conditions around an air-filled cylinder and using a phantom corresponding to a segment of an arm. This prototype demonstrates the possibility of implementing an all-textile antenna, reducing the backward radiation in comparison to the microstrip-based antennas by the use of a substrate-integrated waveguide topology.

INDEX TERMS Antennas, cavity-backed, embroidery, microwave, multifilament yarns, smart textile, threads, wireless, woven structures.

I. INTRODUCTION

During the last decade there has been an overwhelming interest in flexible circuits, especially antennas, based on textile alternatives, thanks to the possibility of integrating them in clothing –such as special garments for firefighters–, upholsteries –sensors based on smart textile– or developing conformable structures. In the literature, a variety of solutions has been developed to implement textile-integrated circuits (TIC). Embroidered techniques [1]–[5], non-woven solutions [6]–[8], designs based on using several fabrics with different electromagnetic behavior [9]–[11] or ink-jet printed patterns over textile substrates [12]–[15] are some of the most cited solutions.

Nevertheless, with the aim of implementing a multilayered antenna fully integrated in textile, the beforementioned alternatives are not convenient due to the following reasons. The conventional embroidery technique and the ink-jet printing procedures do not allow the design of multilayer designs, whereas the use of non-wovens or different fabrics requires additional adhesives or gluing procedures in order to fabricate the prototypes. As a consequence, these options prevent the prototypes from being multilayered, all-textile and available for large scale production simultaneously.

For these reasons, the authors have found weaving technology as an interesting alternative to design and manufacture fully textile integrated circuits [16]–[18]. Nevertheless, with the aim of avoiding the backwards radiation resulting from the microstrip structure already discussed in [16], a novel antenna is presented in this work, whose topology is based on a substrate integrated waveguide (SIW) cavity-backed slot antenna. Although in the literature some approaches to develop textile integrated waveguide (TIW) antennas have already been proposed, they have been manufactured using

previously fabricated conductive fabrics, presenting the disadvantages already mentioned [19]–[26].

Not only the textile SIW antennas presented in the literature have been manufactured using prefabricated conductive fabrics, but also the conductive vias have been implemented using brass eyelets [19], [20], [23], [25], [26], avoiding the complete integration in textile. For this reason, in order to achieve the goal of a complete integration of the antenna into the textile, a mixed embroidered and woven coaxial-fed cavity-backed slot antenna for wireless applications is proposed in this work.

This paper is organized as follows. In Section II, the structure of the antenna is presented. In Section III, the employed materials are characterized. In Section IV, the simulations are performed. In Section V, the fabrication process is discussed. In Section VI, the experimental validation is presented. Finally, conclusions are drawn.

II. STRUCTURE OF THE ANTENNA

A mixed embroidered and woven coaxial-fed cavity-backed slot antenna for wireless applications is proposed for its operation at 5 GHz with a 20% bandwidth. The antenna is based on the SIW technology, for this reason, the structure is divided into three layers: the slotted layer which corresponds to the top cover, the dielectric layer whose thickness is H, and the ground layer which corresponds to the bottom cover of the SIW, as schematically depicted in Figure 1, together with the employed coordinate system.

In order to achieve a cavity structure, as already depicted in Figure 2, one of the ports of the SIW whose length is given by L_A, is short-circuited. The short-circuit is achieved using identical extra conductive vias whose diameters are denoted by D and which are separated S between centers. The antenna is fed using a coaxial cable which is connectorised through the ground layer (or bottom layer) of the SIW using a SMA connector. This connector is placed at a distance d_F from the short-circuit as depicted in Figure 2, corresponding to a quarter of the guided wavelength.

The radiating slot, which is placed in the top layer of the SIW, is a rectangle-shaped slot whose dimensions are L_S and W_S, respectively. With the aim of achieving the required 5 GHz resonant frequency, the slot is placed at a distance d_S, corresponding to a quarter of the guided wavelength, from the other port of the SIW, as depicted in Figure 2, which has also been short-circuited. The beforementioned dimensions are summarized in Table 1.

The proposed antenna is fully integrated in textile and the different layers of the SIW structure are achieved using weaving technology. For this reason, the structure of the woven layers corresponds to the topology already presented in [27] and summarised in Figure 1. The TIW structure presented in Figure 1 is composed of a dielectric layer between two conductive plates. On the one hand, the dielectric materials which conform the substrate are polyethyleneterephthalate (PET) and polyethersulfone (PES) for the warp and the weft directions, respectively. On the other hand, the conductive plates are conformed using *Shieldex 117f17 2-ply* and *Shieldex 117f17 1-ply* yarns for the warp and the weft directions, respectively. In both cases, the warp threads –which are parallel to the warp direction– are previously mounted in the weaving loom, whereas the weft threads –which are parallel to the weft direction– are successively inserted between the upper and lower sheds of warp threads. The employed materials are analysed in the following section.

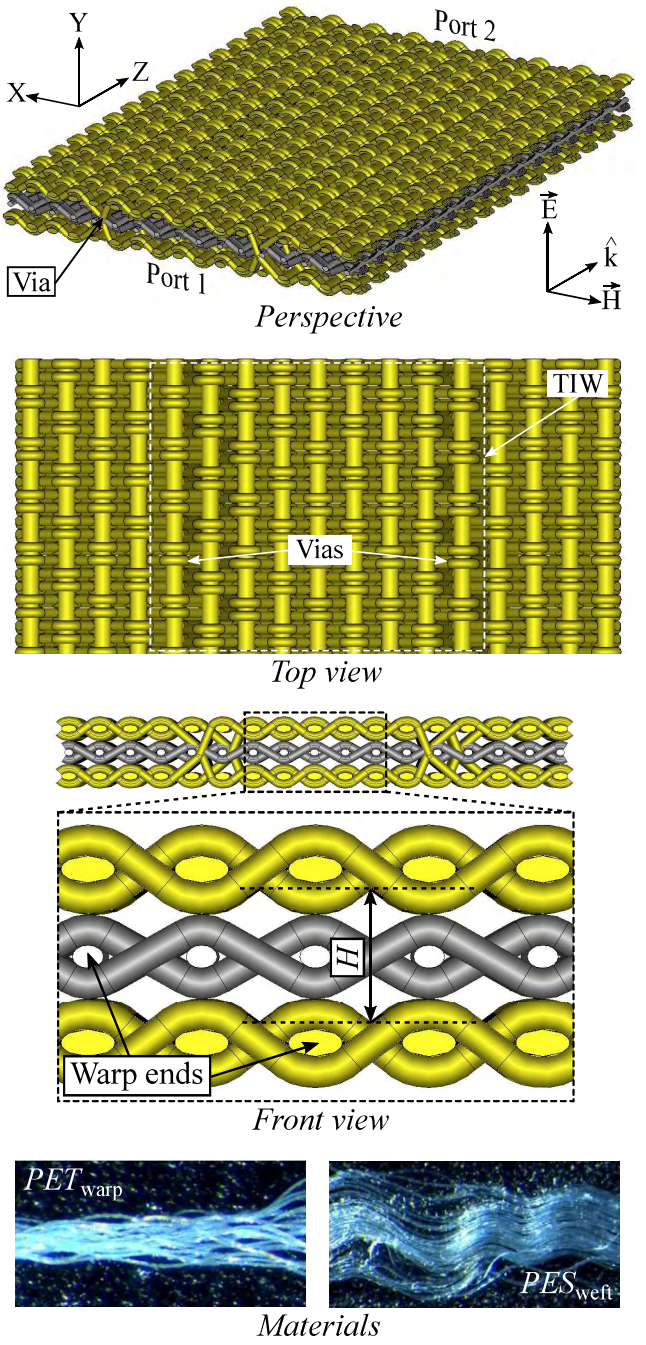

FIGURE 1. Overview of the millimeter-wave TIW proposed in [27], detailed views and materials (threads with their unraveled filaments).

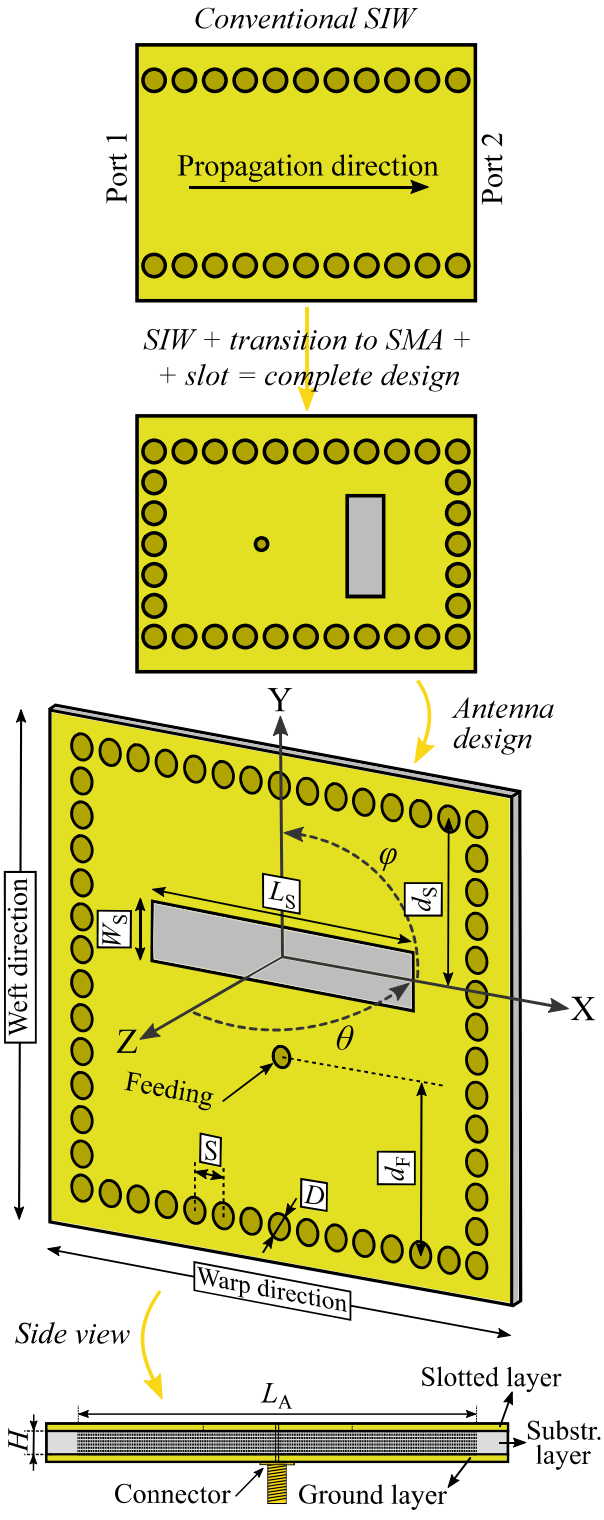

FIGURE 2. Schematic procedure to design of the proposed antenna, general overview, reference coordinates system, dimensions and detail of the radiating slot, and side view with dimensions and identification of the layers.

III. CHARACTERISATION OF THE EMPLOYED MATERIALS

As previously mentioned, the proposed antenna has been designed using two different techniques. On the one hand, the textile structure composed of three layers has been woven. On the other hand, the conductive vias which connect the different layers have been implemented using an embroidery technique.

TABLE 1. Dimensions of the proposed antenna (mm).

L_A	H	D	S	d_F	d_S	L_S	W_S
28	0.36	0.2	0.4	13	13	17	2.8

The woven structure employed in this antenna has been provided from a sample of the woven structure required in the TIW thoroughly discussed in [27]. However, while the woven structure of the TIW presented conductive threads in both the warp and the weft directions, the woven structure employed in this antenna belongs to a part of the sample where the conductive warp threads have been replaced with dielectric warp threads. In other words, the *Shieldex 117f17 2-ply* yarns have been substituted for PET yarns, as in the middle layer. For this reason, it is expected that the gain of the antenna is not very high.

Although the equivalent relative permittivity of the substrate has already been discussed in [27] using a three-step modelling technique, and found to be $\epsilon_{eq} = 1.55$, the operating frequency of the herein presented antenna is much lower. Consequently, in this work, the equivalent relative dielectric permittivity of the proposed structure may increase due to the fact that the air gaps are smaller with respect to the associated wavelength. With the aim of experimentally characterising this value, a TIW provided with a pair of TIW to coaxial transitions has been manufactured and measured using the same textile structure as the antenna. The measurements have been compared to the corresponding simulations of the layers model (LM), while sweeping the value of the ϵ_{eq} parameter.

Figure 3 schematically depicts the TIW provided with the aforementioned transitions. Both feeding points are located at a distance d_{F1} and d_{F2}, respectively, from the shortcircuiting vias. Both distances are $d_{F1} = d_{F2} = 12$ mm, while the length and width of the waveguide are $L_T = 30$ mm and $W_T = 28$ mm, respectively. The dimensions of the conductive vias and their separation are analogous as in the previously described design of the antenna.

The TIW has been manufactured and connectorised as depicted in Figure 4, and then measured using an Agilent N5247A PNA-X vector network analyser. A narrow-band performance of the TIW could be anticipated due to the design of the transitions. However, the main goal is finding the central frequency of the manufactured TIW bandpass, which has been found to be $f_{cBP} = 5.6$ GHz.

Different versions of the LM associated to the TIW have been simulated sweeping the value of the ϵ_{eq} and $\tan(\delta)_{eq}$ parameters, respectively. Eventually, $\epsilon_{eq} = 2.2$ and $\tan(\delta)_{eq} = 0.01$ have been found to be the values of the equivalent relative permittivity and loss tangent which make the simulations and measurements coincide, as depicted in Figure 5.

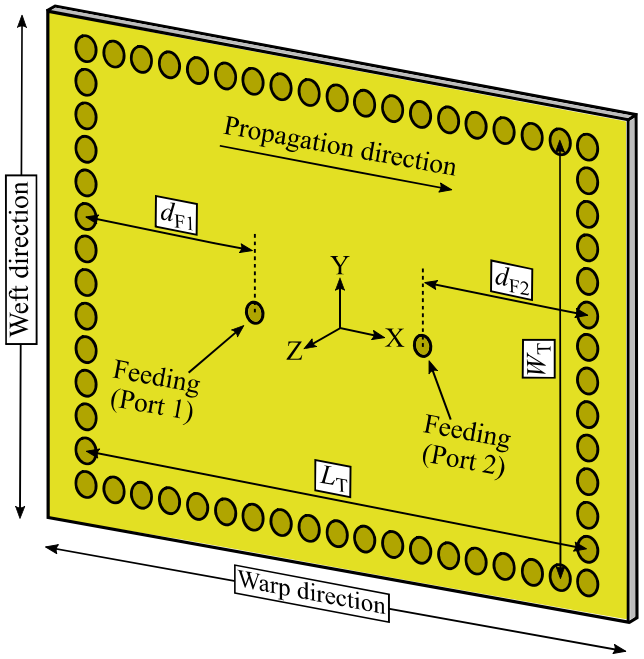

FIGURE 3. Schematic design of the TIW provided with a pair of TIW to coaxial transitions.

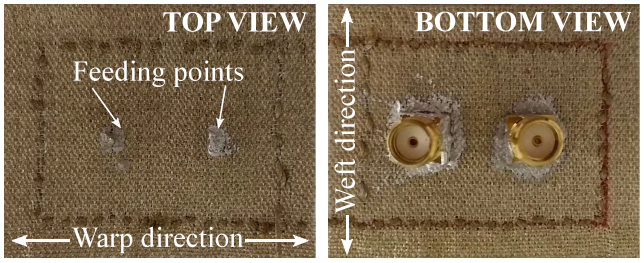

FIGURE 4. Manufactured TIW provided with a pair of TIW to coaxial transitions: top and bottom views.

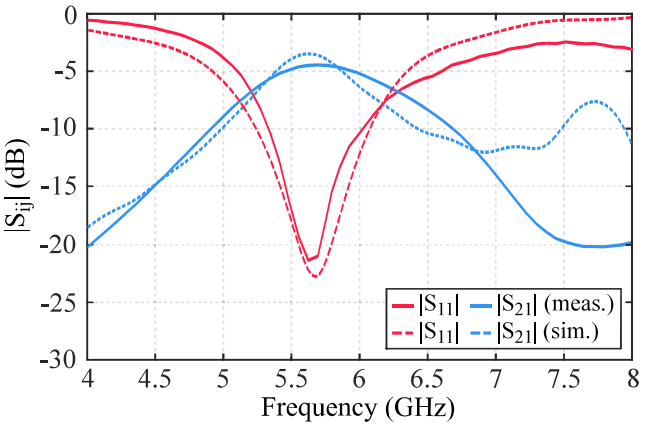

FIGURE 5. Simulated and measured scattering parameters of the TIW and corresponding transitions to coaxial.

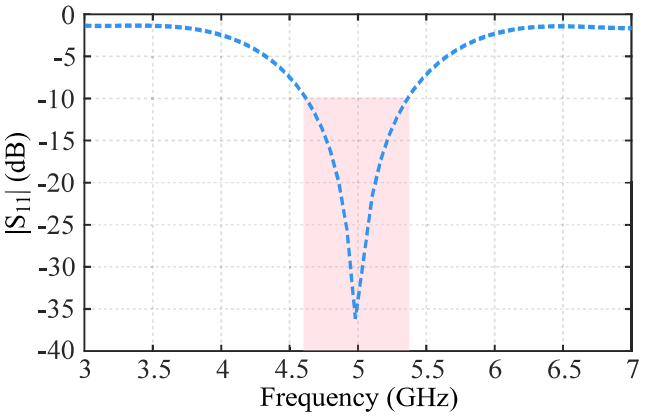

FIGURE 6. Simulated magnitude of the reflection coefficient (dB) and bandwidth (shaded) of the antenna.

Consequently, as predicted, the equivalent relative permittivity has increased. The obtained values of these parameters have been found to be coherent in comparison to measured values of these parameters beloging to different textile substrates in the literature [28], [29]. Employing the same procedure, the equivalent electrical conductivity has been found to be $\sigma_{eq} = 2 \cdot 10^4$ S/m. This poor value of conductivity is translated into the value of the transmission loss of 1.5 dB/cm, as can be seen in Figure 5.

IV. SIMULATIONS

Once the materials have been characterized, the mixed embroidered and woven cavity-backed slot antenna has been designed and simulated. The LM corresponding to the proposed design has been analysed using a 3D high frequency electromagnetic simulator and a FDTD solver. The complete antenna cannot be simulated using the monofilament model (MM), due to the computational resources required. The same problem happened with the mentioned TIW to characterize the woven structure, both structures are composed of numerous threads. The MM can be employed in woven structures when they are composed of a reduced number of threads due to the fact that they operate at higher frequency ranges –as occurs in Figure 1– or because the threads are thicker and less threads are required to conform the woven structure.

In order to feed the antenna, a short 50 Ω–impedance coaxial cable has been simulated, one of its ports has been connected to the antenna as presented in Figure 2 as if it were a SMA connector. In the second port of this coaxial cable, a waveguide port has been defined to excite the electromagnetic field in the coaxial cable and, correspondingly, in the antenna.

Figure 6 depicts the simulated magnitude of the reflection coefficient (dB) and bandwidth (shaded) using the LM. Figure 7 represents the definition of the *E*–plane and the *H*–plane of the proposed antenna, whereas Figure 8 depicts the simulated normalized radiation patterns: *E*–plane and *H*–plane, including both co-polar (CP) and cross-polar (XP) contributions.

The simulated values of the gain, directivity and total efficiency are $G_S = -5.1$ dB, $D_S = 6.3$ dB and

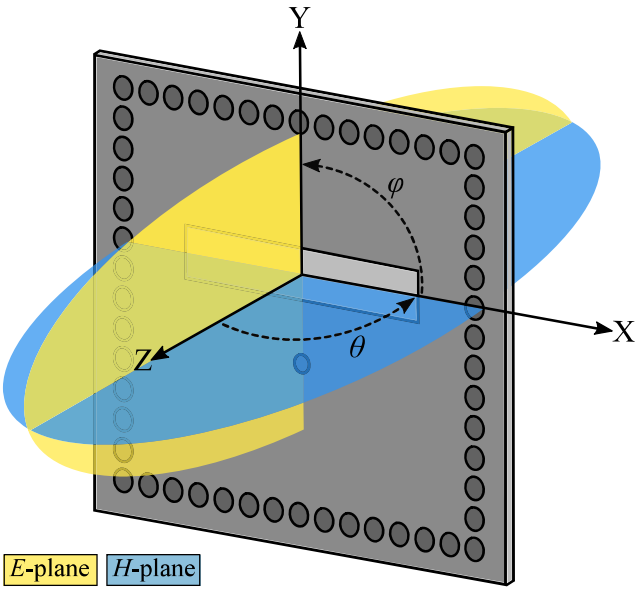

FIGURE 7. Definition of the *E*–plane and the *H*–plane.

$\epsilon_{\text{eff\_S}} = 7.2\%$, respectively. The negative value of the simulated gain is, essentially, due to the low value of the equivalent conductivity. This low value is the result of using conductive material only for the warp threads, instead of for the warp and the weft threads.

A. ADDITIONAL SIMULATIONS

The antenna has been additionally simulated under different conditions. First, the antenna has been bent around a air filled cylinder whose radius is denoted by R_{C}, as schematically represented in Figure 9. This condition is important to analyses, as the antenna will be manufactured using non-rigid materials and its flatness cannot be ensured. Additionally, in Figure 9, the coaxial cable employed to feed the antenna is also represented.

Secondly, a phantom corresponding to a segment of an arm has been developed for the corresponding simulations, as schematically represented in Figure 10. The segment of the arm consists of the intersection between to circumferences whose radius is given by $R_{\text{M}} = 50$ mm, and a rectangle whose thickness is denoted by $T_{\text{M}} = 10$ mm. The resultant surface has been extruded a length given by the $L_{\text{M}} = 100$ mm, the length of the segment of the arm. The arm phantom is also composed of the corresponding bones, the radius and the ulna. The cross-sections of both bones have been approximated by two elliptic circumferences. The corresponding radii of the radius bone are $R_{\text{RX}} = 7$ mm and $R_{\text{RZ}} = 5$ mm, respectively, whereas the radii of the ulna bone are given by $R_{\text{UX}} = 9$ mm and $R_{\text{UZ}} = 6$ mm, respectively. Both bones are separated a distance $D_{\text{B}} = 23$ mm between their centers. The most relevant characteristics of the materials which compose the phantom, from $f_{\text{min}} = 3$ GHz to $f_{\text{max}} = 7$ GHz, are summarised in Table 2.

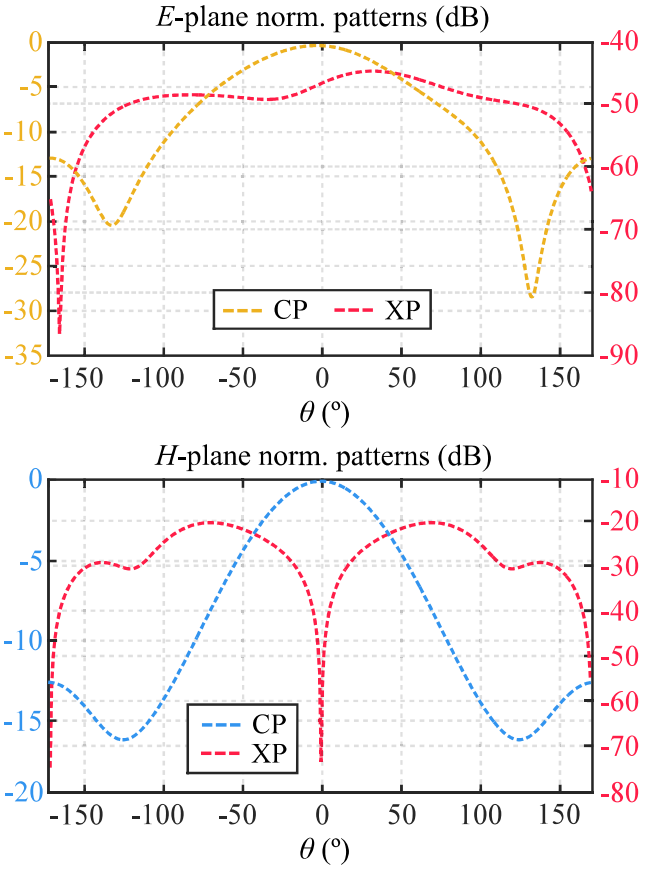

FIGURE 8. Simulated normalized radiation patterns of the antenna: *E*–plane and *H*–plane.

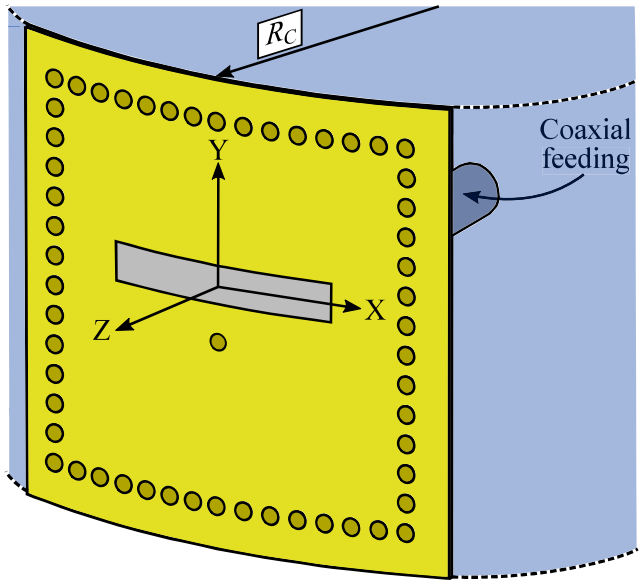

FIGURE 9. Schematic set-up corresponding to the radius of curvature (R_C) of the antenna.

In Figure 11, the simulated magnitude of the reflection coefficient of the antenna in different scenarios is represented. The $|S_{11}|$ parameter is slightly deteriorated when the antenna

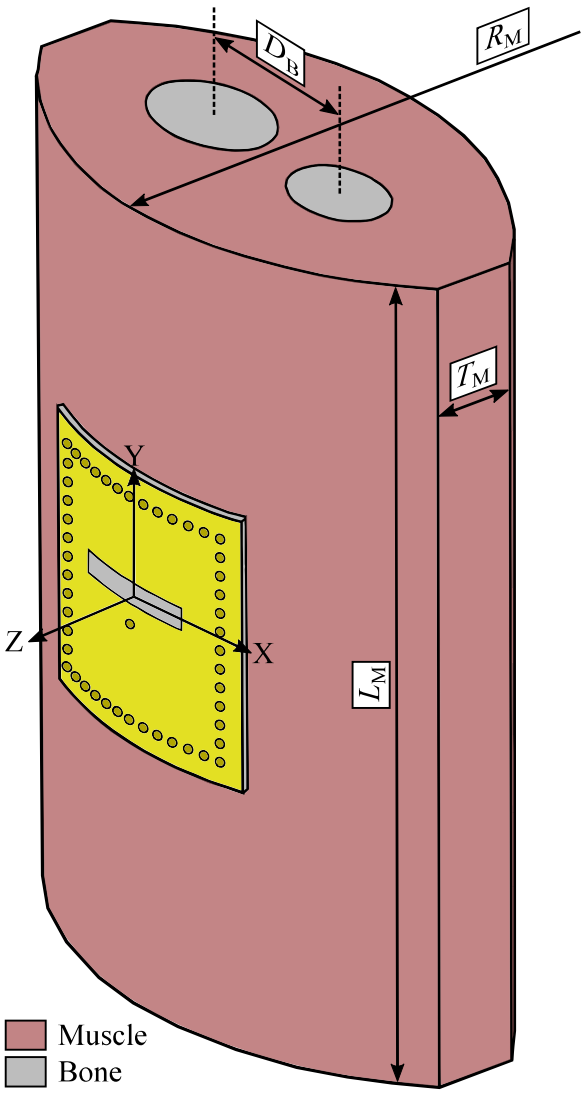

FIGURE 10. Schematic set-up corresponding to an arm phantom and the antenna and definition of the materials.

TABLE 2. Characteristics of the materials which compose the phantom [30]–[34].

Material	ε_r at f_{min}	ε_r at f_{max}	μ_r	Density (Kg/m^3)
Muscle	51.83	44.19	1	1041
Bone	10.99	8.65	1	1850

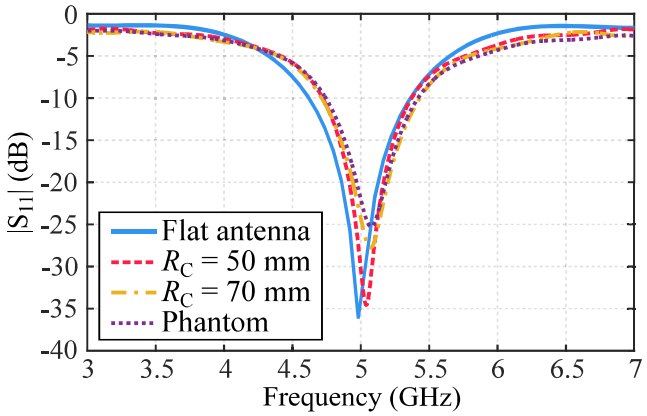

FIGURE 11. Simulated magnitude of the reflection coefficient in different scenarios: flat antenna, R_C and phantom.

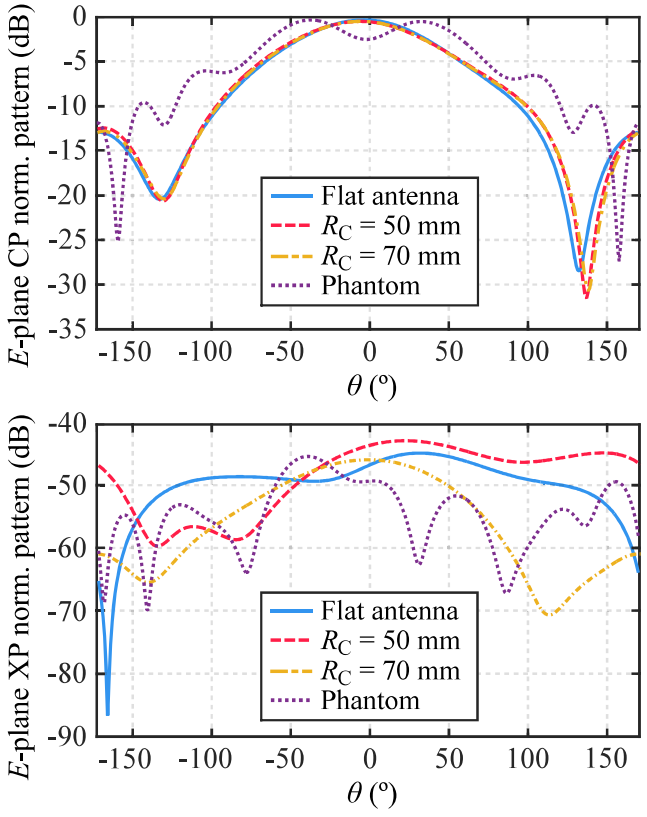

FIGURE 12. Simulated normalized *E*–plane radiation patterns in different scenarios: flat antenna, R_C and phantom.

is bent a radius R_C, the greater the radii, the more deteriorated the performance of the antenna will be. When the antenna is put over the mentioned phantom, the $|S_{11}|$ parameter is modified from −35 dB (flat antenna) to −25 dB (antenna over the phantom). Nevertheless, $|S_{11}| = -25$ dB still represents a good performance of the antenna.

Figure 12 depicts the simulated *E*–plane normalized radiation patterns corresponding to the already mentioned different scenarios. Both the CP and XP contributions have been normalized using each corresponding maximum value of each CP contributions. The CP contributions present the maximum at $\theta = 0°$ except in the simulation over the phantom, in which the directivity is reduced 2.5 dB at $\theta = 0°$. The XP contributions are at least 40 dB below the CP contribution at $\theta = 0°$ for all the different scenarios.

Alternatively, Figure 13 represents the simulated *H*–plane normalized radiation patterns corresponding to each of the mentioned scenarios. The normalization procedure has been analogous to the one already explained for the *E*–plane.

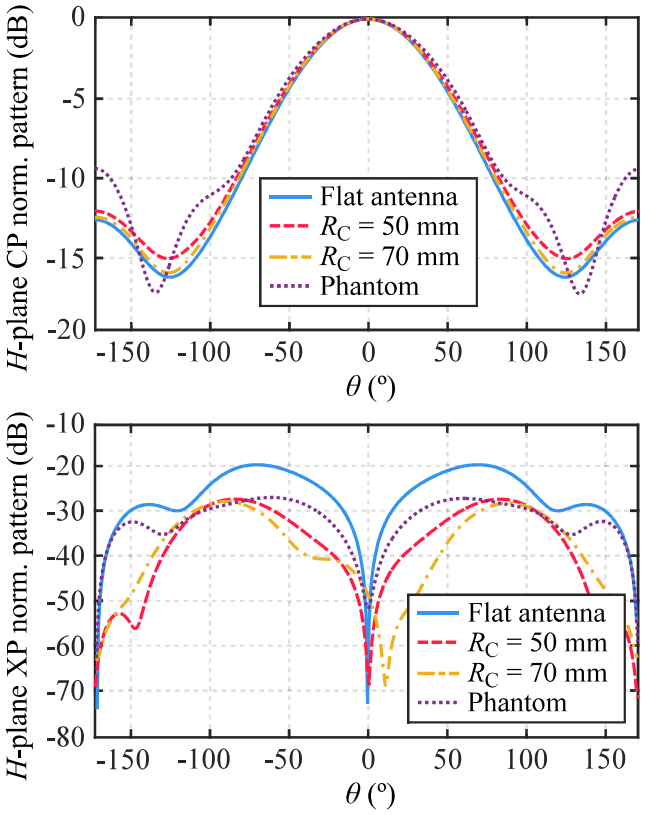

FIGURE 13. Simulated normalized *H*–plane radiation patterns in different scenarios: flat antenna, R_C and phantom.

The CP contributions present similar values for the different scenarios except for the one using the phantom, in which the value of the radiation pattern in the backward direction ($\theta = 180°$) has increased almost 6 dB. The XP contribution decreases for every value of the angle θ when the antenna is analysed under the bent conditions or using a phantom. Figure 14 depicts the simulated 3D radiation pattern corresponding to the antenna over the phantom in which the reduction of the mentioned 2.5 dB at $\theta = 0°$ for the *E*–plane can be easily identified.

V. FABRICATION PROCESS

A fully textile integrated antenna has been manufactured using three processes. First, the woven structure composed of three layers has been manufactured using an industrial loom. Secondly, an embroidery process has been employed to manufacture the conductive vias. Finally, a cutting process has been required to fabricate the radiating slot. Once the antenna is fabricated, it is connectorised using a SMA connector which is glued to the textile prototype employing conductive epoxy glue.

The woven structure is composed of three layers. The middle layer is completely dielectric, however, the conductive covers of the TIW structure have been manufactured using conductive weft threads and dielectric warp threads. This is due to the woven structure employed to fabricate the proposed antenna has previously designed and employed for another

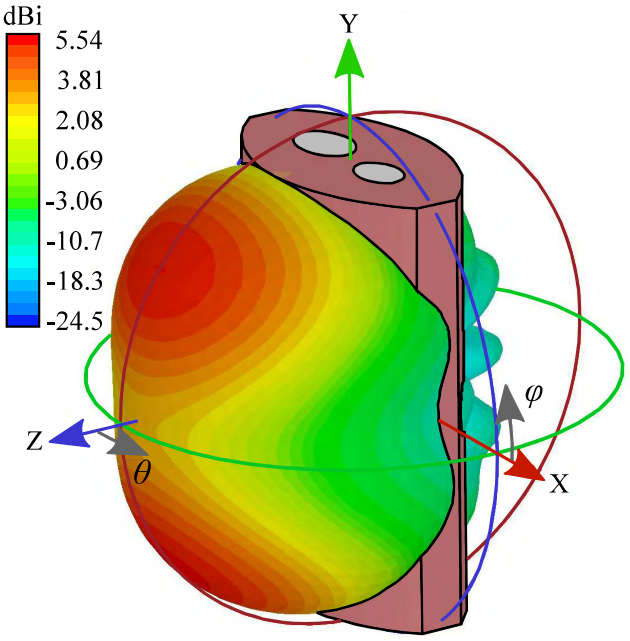

FIGURE 14. Simulated 3D radiation pattern corresponding to the antenna over the phantom (directivity).

purpose. Figure 15 depicts several schematic drawings of the woven structure. In Figure 15a, a side view of the woven structure is presented, where the warp ends and the weft threads are depicted. Figure 15b represents the side view of the woven structure after cutting the threads belonging to the radiating slot using a laser prototyping machine LPKF ProtoLaser. To avoid the presence of loose threads after the cutting process, the woven structure has been manufactured using dielectric binders, as depicted in Figure 15c.

Cutting the radiating slot using a laser prototyping machine has been decided due to the unavailability to use a weaving loom provided with an automatic cutting mechanism and an auxiliary layer.

The conductive vias of the prototype are achieved using an embroidery procedure with a Brother Innovis NV2600 embroidery machine. The conductive thread which emulates the conductive vias has been schematically represented in Figure 15d, in which it is embroidered in the woven structure. As a result, Figure 16 depicts the manufactured prototype. Figure 16a and Figure 16b represent, respectively, the top and bottom views of the prototype before its connectorisation. Analogously, Figure 16c and Figure 16d depict the top and bottom views of the manufactured prototype after the connectorisation.

Figure 17 depicts detailed views of the manufactured prototype and corresponding magnifications. In Figure 17a, the conductive cover of the woven SIW structure is depicted, in which the conductive warp threads and the dielectric weft threads can be identified. Figure 17b represents the woven substrate, whereas Figure 17c depicts a side view of the prototype where the three layers can be easily identified.

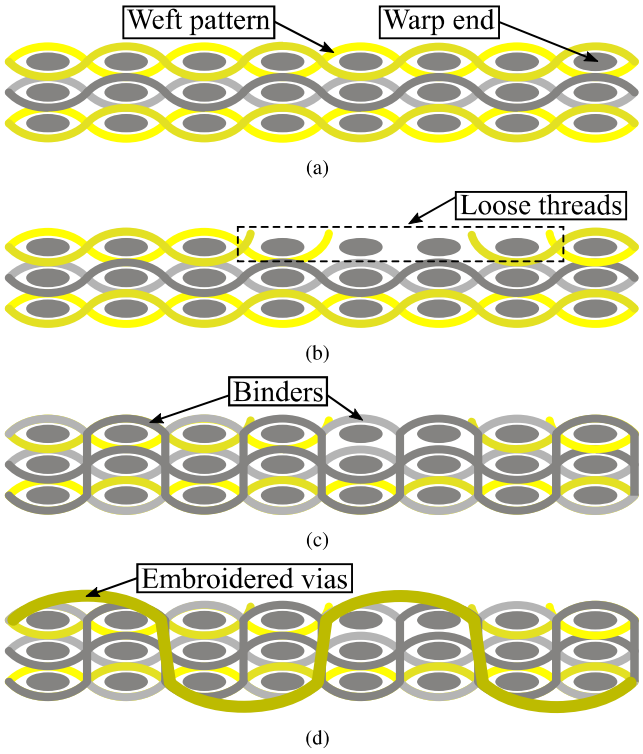

FIGURE 15. Schematic drawing of the woven structure. (a) Side view. (b) Side view after cutting the threads belonging to the radiating slot. (c) Side view using binders to avoid the loose threads. (d) Side view and conductive thread which emulates the embroidered vias.

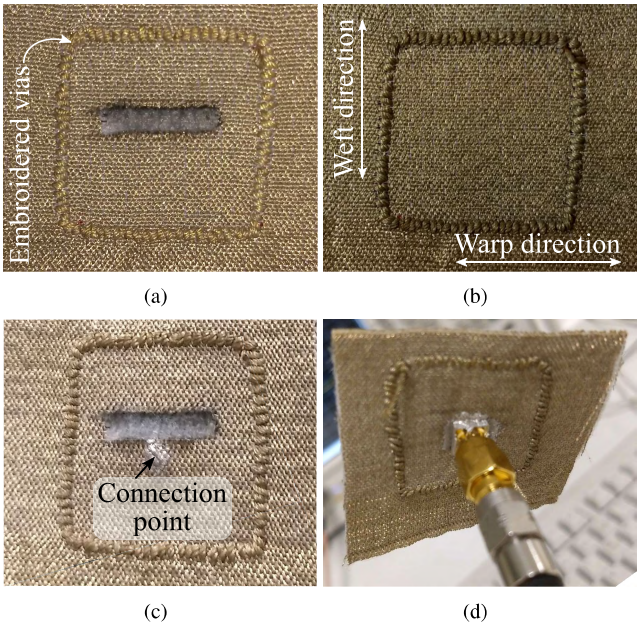

FIGURE 16. Manufactured prototype. (a) Top view before connectorising. (b) Bottom view after connectorising. (c) Top view after connectorising. (d) Bottom view after connectorising.

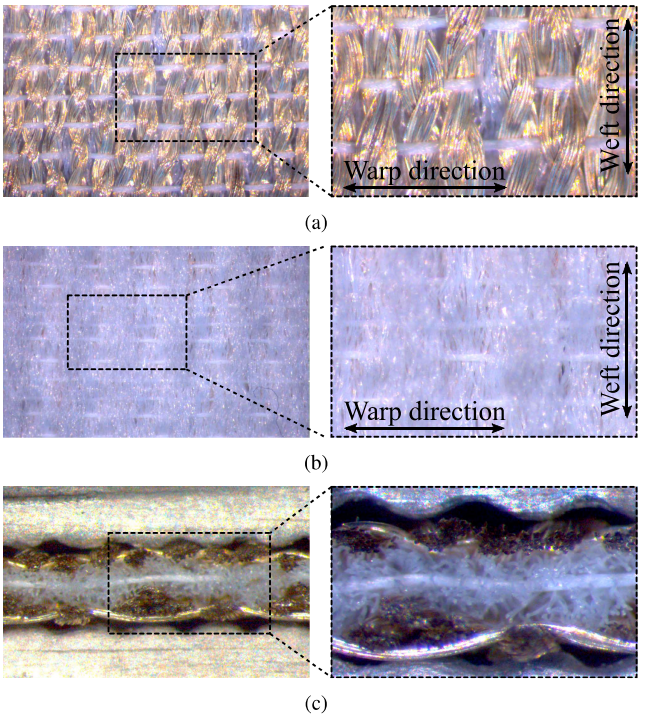

FIGURE 17. Detailed views of the manufactured prototype and magnifications. (a) Conductive cover of the TIW structure. (b) Substrate. (c) Side view.

A. POSSIBLE IMPROVEMENTS FOR THE PROTOTYPE

Although this paper presents a first approach to develop a TIW based antenna for wireless applications, the prototype can be enhanced. For this purpose, four important modifications can be taken into account if access to a special jacquard loom is possible.

First, the conductive plates which conform the SIW structure can be achieved using conductive threads in both directions –warp and weft–. For this purpose, the assembly of the industrial loom must be updated, by the use of warp conductive threads. The procedure of changing the assembly of an industrial loom is very costly, for this reason, this prototype has been developed using an already manufactured woven structure for a different application.

Second, although related to the previous one, the loss corresponding to the dielectric materials can be reduced by the use of less dense woven structures and taking advance of the almost lossless propagation through the air.

Third, the conductive vias could be manufactured employing new woven patterns, avoiding the necessity of the embroider procedure. To do this, conductive weft threads must connect the three different layers of the woven structure.

Finally, the radiating slot can be achieved during the same weaving process avoiding the use of an external machine such as the prototyping laser machine. In order to do this, an *ad hoc* industrial jacquard loom provided with a cutting mechanism is required. As a consequence, when the path of a conductive thread has to be interrupted in order to generate the radiating slot, this thread continues its path through an auxiliary layer –a dummy layer– which is located above the top layer. Afterwards, in the same industrial loom,

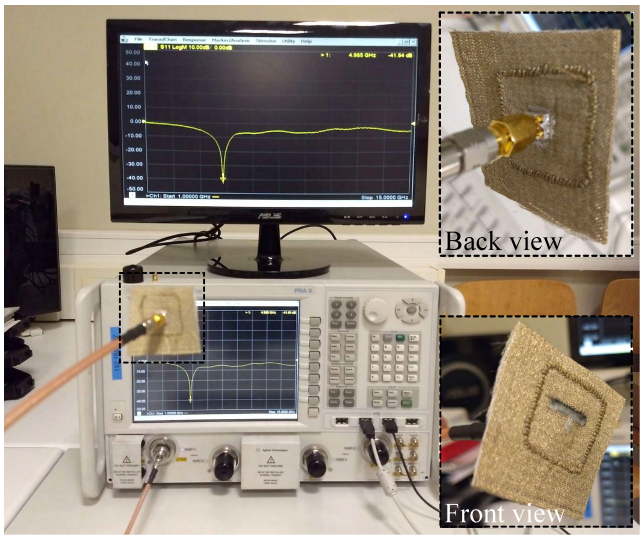

FIGURE 18. Measurement set-up with PNA-X and magnifications of prototype under test.

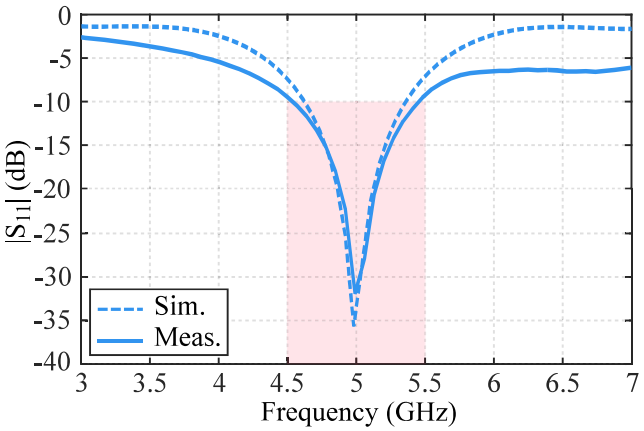

FIGURE 19. Simulated and measured magnitude of the reflection coefficient (dB) and bandwidth (shaded).

a cutting mechanism eliminates the auxiliary layer be cutting in between the dummy and the top layers. This procedure is similar to the one used in order to manufacture the velvet fabrics.

VI. EXPERIMENTAL VALIDATION

With the aim of experimentally validating the prototype, the reflection coefficient has been measured using an Agilent N5247A PNA-X vector network analyser with the set-up presented in Figure 18. The measured reflection coefficient has been compared with the simulations, as depicted in Figure 19. The manufactured antenna operates at a central frequency of 5 GHz and the measured bandwidth has been found to be equal to 20%.

The manufactured prototype has been measured in a spherical range in anechoic chamber in order to characterize its radiation pattern, directivity, gain and total efficiency. The measurements have been conducted at the frequency

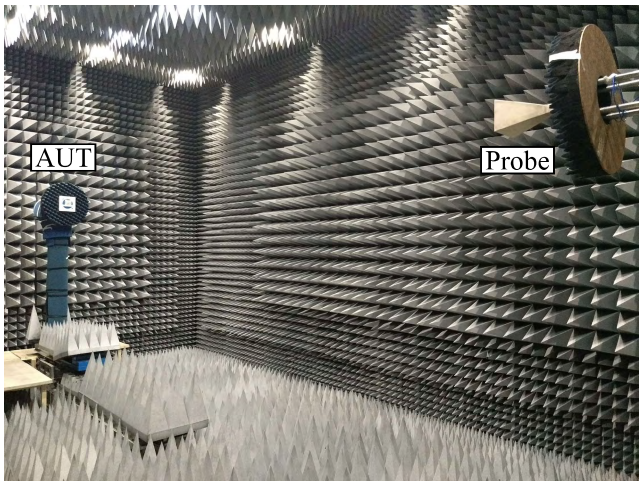

(a)

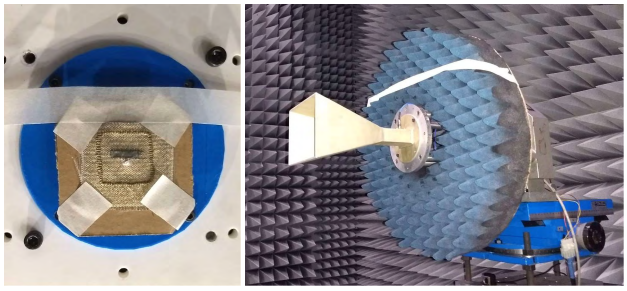

(b) (c)

FIGURE 20. Measurement set-up in anechoic chamber. (a) Overview of the set-up. (b) Detailed antenna under test (AUT). (c) Detailed probe antenna.

$f_o = 5$ GHz, which corresponds to the $|S_{11}|$ minimum, as observed in Figure 19.

The radiation pattern of the textile antenna under test (AUT) has been measured at the distance of $R = 5.4$ m, which is in the far field region. Figure 20a represents the measurement set-up at the spherical range in anechoic chamber, where the AUT has been mounted in a cardboard and plastic platform as detailed shown in Figure 20b, and the probe antenna is a Narda 643 SGH [35]. The *E*-plane and *H*-plane normalized radiation patterns of the AUT have been measured. The measurements have been processed using ANCAN software [36], [37] and compared with the simulated data, as depicted in Figure 21.

A good agreement between simulated and measured CP components can be noticed. The difference between the simulations and measurements of the *E*-plane can be due to a fabrication defect in the slot, which is not exactly rectangle-shaped as required, as it can be perceived in Figure 16a and Figure 16c. Additionally, this anomaly can be noticed in both the CP and the XP contributions, for the same range of angles.

However, in both *E*-plane and *H*-plane measured radiation patterns, the backward radiation is reduced in comparison to the simulations up to 10 dB and 20 dB for the *E*–plane and *H*–plane, respectively. The measured XP components present

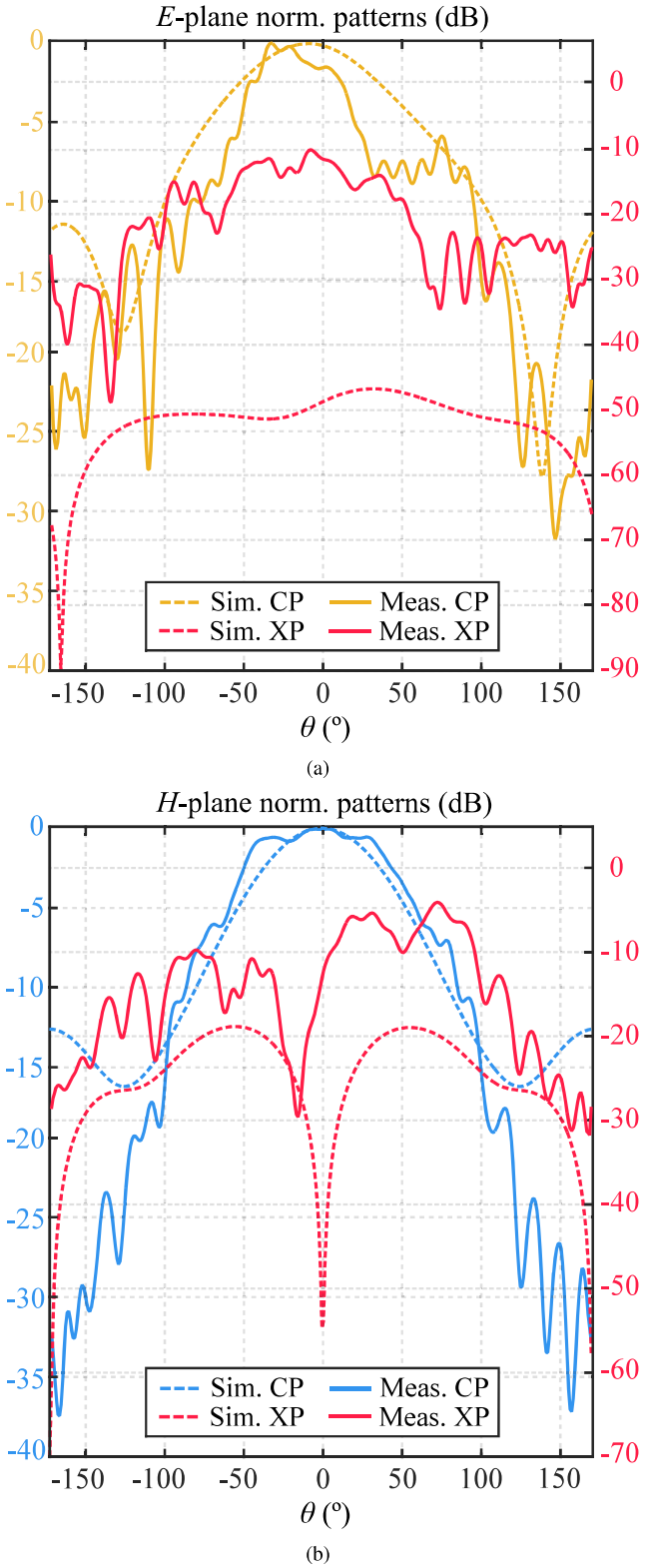

FIGURE 21. Simulated and measured normalized radiation patterns. (a) *E*–plane. (a) *H*–plane.

higher levels in comparison to simulations, especially in the *E*-plane. This could be due to the fact that the simulations are done using an homogeneous conductive material, although

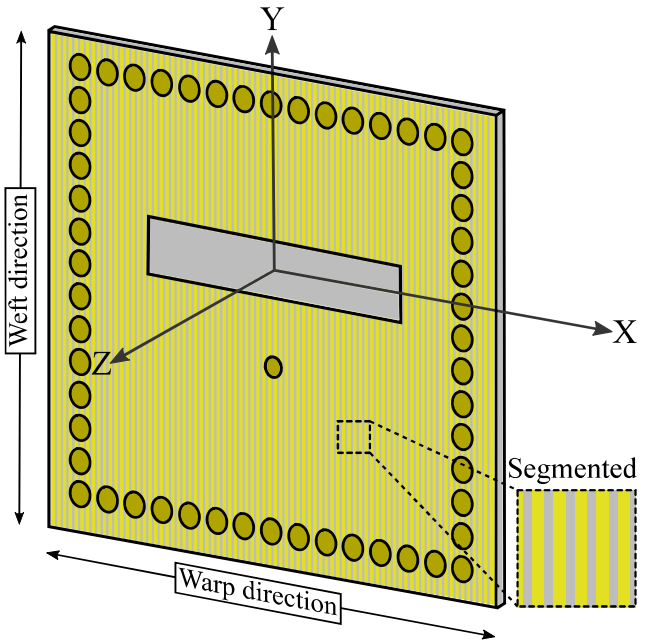

FIGURE 22. Schematic design of the proposed antenna using segmented conductive plates and corresponding magnification.

the manufactured antenna has been developed using conductive threads only in one direction, and the contact between these weft threads cannot be guaranteed. As a result, there is not any path for currents parallel to the warp direction, modifying the flow of the currents in comparison to standard SIW antennas. Nevertheless, a difference of 15 dB between the measured CP and the measured XP contributions for the *E*–plane has been considered to be an acceptable result for this novel antenna. Additionally, the measured XP contribution of the *H*–plane seems to have been slightly shift during the measuring procedure, as its minimum value does not correspond to $\theta = 0°$, but to $\theta = -15°$, avoiding a difference between the CP and the XP contributions of 30 dB at the direction corresponding to maximum radiation.

In order to demonstrate that the reason why there is so much difference between the values of the simulated and measured XP contributions is the lack of contact between the weft conductive threads, new simulations have been realized. For this purpose, the conductive covers of the simulated antenna have been substituted by segmented covers which emulate the conductive weft threads without contact between each other, as schematically depicted in Figure 22. As a result, in Figure 23, the original simulations, the measurements and the new simulations have been compared. As a consequence, the difference between the new simulations and the measurements has been reduced. Additionally, the measurements have been repeated after up to five washing cycles of the prototype, providing the same results. As a consequence, the prototype can be considered washable.

Directivity has been calculated by integrating the measured AUT radiation pattern, yielding to $D_{\mathrm{M}} = 7.49$ dB, which is in agreement with the low directivity of the AUT radiation pattern (as confirmed by the normalized directive gain

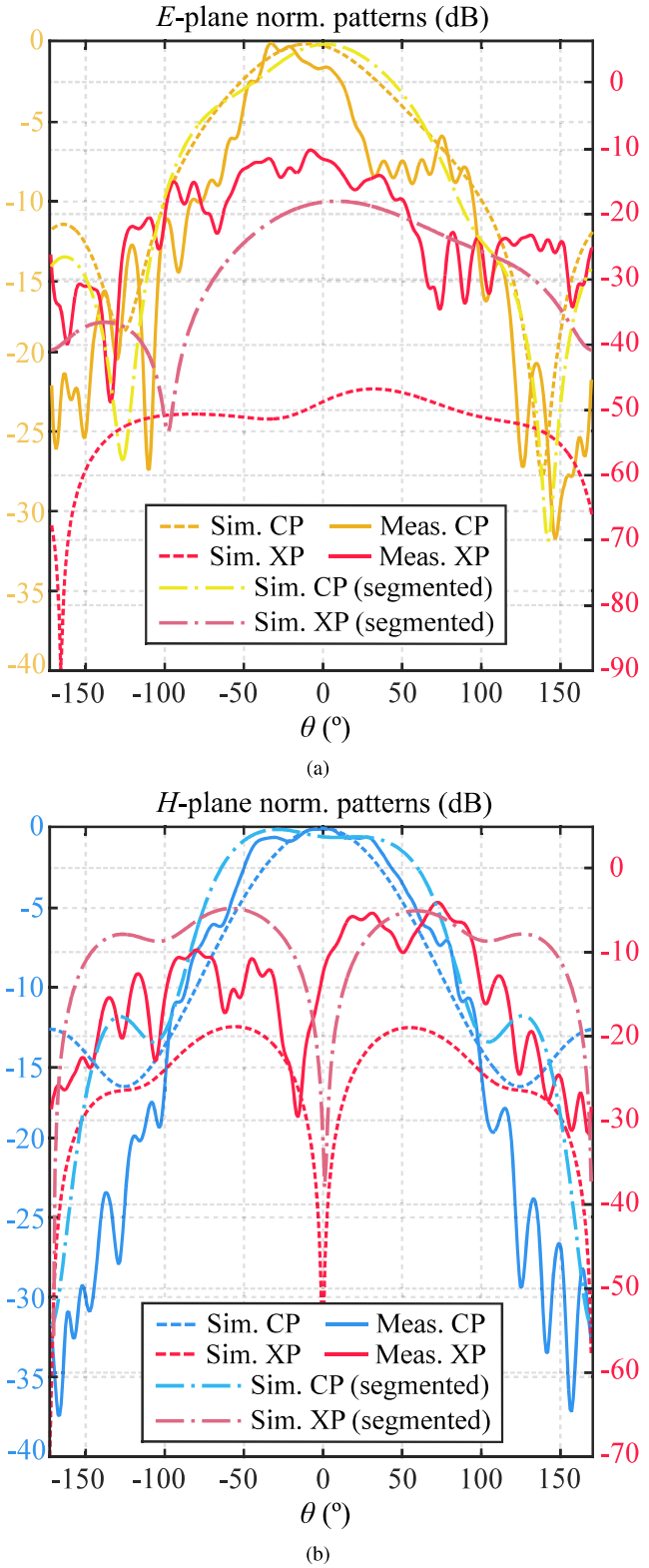

FIGURE 23. Simulated and measured normalized radiation patterns compared to the simulations using the segmented antenna. (a) *E*–plane. (a) *H*–plane.

pattern depicted in Figure 24). Analogously, Figure 24 also depicts the measured normalized gain pattern in the backward direction.

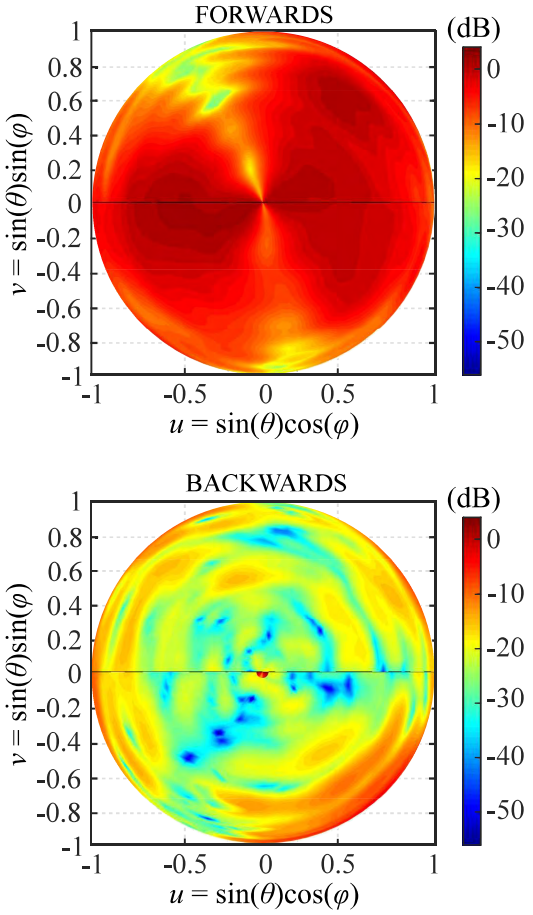

FIGURE 24. Measured normalized gain patterns: forwards and backwards, respectively.

TABLE 3. Comparative between simulations and measurements.

Parameter	Gain (dB)	Directivity (dB)	ε_{eff}
Simulated	-5.1	6.3	7.2%
Measured	-4.9	7.49	5.77%

AUT gain has been calculated by means of the inter-comparison technique [38], leading to $G_M = -4.9$ dB. Finally, given the AUT gain and directivity, the AUT total efficiency can be calculated: $\epsilon_{eff\_M} = 5.77$ %. A comparative between the simulated and the measured values of the gain, directivity and total efficiency is summarised in Table 3.

A comparative between different textile SIW antennas found in the literature has been summarised in Table 4 in terms of the operating frequency, f, bandwidth, BW, gain, G, directivity, D, and efficiency, ϵ_{eff}. In the case a parameter has not been provided in the corresponding paper, NP has been indicated instead. The antennas presented in [19], [20], and [23]–[25] present higher efficiencies for several reasons. The main reason is due to their operating at lower frequencies than the antenna proposed in this section. Moreover, in the

TABLE 4. Comparative between textile SIW antennas in the literature.

Ref.	f (GHz)	BW (%)	G (dB)	D (dB)	ε_{eff} (%)
[23]	2.45	6.12	5.35	NP	74.3
[21]	5.8	4.3	3.12	NP	37.7
[22]	2.45	6.4	2.9	NP	NP
	5.5	12.1	5	NP	NP
[19]	2.45	4.9	5.9	NP	74
[20]	2.45	12.2	6.5	NP	73
[24]	2.4	16.2	4.7	NP	67
[25]	5.15-5.85	23.7	4.3	NP	85
[26]	2.45	NP	5	NP	89
	2.53	NP	5	NP	93
This	5	20	-4.9	7.49	5.77

TABLE 5. Comparative between other works.

Ref.	f (GHz)	BW (%)	G (dB)	D (dB)	ε_{eff} (%)
[16]	5.9	9.3	-2.75	4.9	17.2
This	5	20	-4.9	7.49	5.77

beforementioned references, the conductive covers of the SIW structure of the antennas are achieved using different conductive fabrics (*ShieldIT Super* from *LessEMF Inc.*) in [23], electrotextile in [19] and [24], conductive copper plated taffeta fabric in [20] and [26]), instead of woven patterns. In [22], even though two different values of the gain are presented, for each frequency band, neither the directivity nor the efficiency are provided, consequently, the antenna is not completely characterized.

In [25], a SIW antenna has been presented which is based on the same topology as the antenna presented in this paper. However, although the antenna presented in [25] has been fabricated using copper-plated taffeta electro-textile, it is not fully integrated into textile for several reasons. Firstly, the employed substrate is cork and, secondly, the conductive vias are achieved using brass eyelets. Moreover, the conductive taffeta and the cork substrate require an additional adhesive procedure to achieve a compact prototype.

In a nutshell, the antenna presented in this paper is a novel completely-textile prototype. As a consequence, gluing procedures, the use of prefabricated commercial conductive fabrics or the use of eyelets have been avoided for its fabrication. The proposed antenna presents a 20% bandwidth, the second highest in comparison to other alternatives in the literature, as summarised in Table 4. The low value of the gain of the proposed antenna has been fundamentally attributed to the use of conductive materials only in one direction. Nevertheless, this issue could be solved, enhancing the performance of the antenna notoriously.

The antenna presented in this paper has also been compared to a previous work developed by Alonso-González *et al.* [16], which is a woven antenna, although it has not been designed using a SIW topology, but a microstrip structure. This comparison is summarised in Table 5. Due to the fact that the antenna presented in [16] is based on a microstrip structure, provided with a radiating slot in the ground plane, the microstrip line presents inherent radiation as it is not a stripline. For this reason, the radiation pattern of this antenna results not only in the desired radiation in the forward direction, but also in undesired radiation in the backward direction. As a consequence, the radiation patterns have only been represented in [16] from $\theta = -90°$ to $\theta = 90°$.

Precisely, due to the undesired radiation in the backward direction in the prototype presented in [16], in this paper, the topology has been changed and a SIW structure has been employed. The SIW structure is provided with two parallel conductive plates so that the plate which is not the one with the radiating slot, behaves as the ground plane, avoiding the radiation in the backward direction, as can be seen in the simulated and measured radiation patterns in Figure 21 and in the representations of the measured normalised gain patterns in Figure 24.

Another fundamental difference between the antenna presented in [16] and the antenna presented in this paper is the feeding. Whereas the antenna in [16] is fed using a SMA connector through the side of the woven fabric –using two little shims of brass–, in this work, the antennas has been connectorised perpendicularly to the woven fabric. Although this could seem a little modification at first, in terms of wearable antennas, this is fundamental. The woven antennas are thought to be completely integrated in textile and, for this reason, the fabrics must not be interrupted to insert a connector, as happened in [16], because the smart garment in which the antenna would be supposed to be integrated would not be a continuous fabric. Nevertheless, the antenna presented in [16] was the first approach to a woven antenna, and these fundamental details have not been taken into account, as the important goal was to demonstrate the radiation phenomenon using a woven structure.

VII. CONCLUSIONS

A novel mixed embroidery and woven coaxial-fed cavity-backed slot antenna for its use in wireless applications has been presented. First, a complete characterization of the employed textile materials has been explained. Then, a translation from a conventional SIW antenna into an embroidery and woven prototype has been presented. To validate the design, a prototype has been manufactured and experimentally characterized. The simulations have been compared to the measurements and a good agreement has been achieved.

Additionally, the antenna has been simulated using different scenarios. First, the performance of the antenna has been analysed bending it around an air-filled cylinder, as it is a flexible prototype. Then, the antenna has been analysed over a

phantom corresponding to a segment of an arm. The phantom has been composed of materials which simulate muscles and bones. The performance of the antenna in these different circumstances has been found to be similar, thus the antenna could be used as a wearable device. In order to find a more realistic simulation set-up of the antenna, a segmented model of the antenna has been studied, in which the conductive covers have been substituted by segments of conductive and dielectric material in order to emulate the conductive threads in the weft direction.

As previously commented, the efficiency of the antenna could be significantly improved by using conductive threads in both the warp and the weft directions. Nevertheless, the authors have not had access again to an industrial loom to repeat the sample. Besides, substituting the warp threads in an industrial loom represents a very costly task which takes several days. For this reason, the purpose of this paper is to demonstrate the possibility of implementing an all-textile antenna, reducing the backward radiation, by the use of a SIW topology.

In addition, the prototype can be enhanced by manufacturing a completely woven TIW antenna by replacing the embroidered vias by new woven patterns using conductive threads. By doing this, the embroider procedure can be eliminated and, consequently, the cost and time employed to manufacture the antenna can be reduced. Additionally, the radiating slot can be achieved during the weaving process using an *ad hoc* jacquard loom provided with a cutting mechanism, avoiding the cutting process with the additional prototyping laser machine. Nevertheless, this work has been only focused on the novel idea of developing the all-textile TIW based antenna and demonstrating its potential application.

REFERENCES

[1] G. Ginestet *et al.*, "Embroidered antenna-microchip interconnections and contour antennas in passive UHF RFID textile tags," *IEEE Antennas Wireless Propag. Lett.*, vol. 16, pp. 1205–1208, Nov. 2017.

[2] A. Paraskevopoulos, D. de S. Fonseca, R. D. Seager, W. G. Whittow, J. C. Vardaxoglou, and A. A. Alexandridis. "Higher-mode textile patch antenna with embroidered vias for on-body communication," *IET Microw., Antennas Propag.*, vol. 10, no. 7, pp. 802–807, May 2016.

[3] A. Kiourti, C. Lee, and J. L. Volakis, "Fabrication of textile antennas and circuits with 0.1 mm precision," *IEEE Antennas Wireless Propag. Lett.*, vol. 15, pp. 151–153, May 2015.

[4] Z. Wang, L. Zhang, Y. Bayram, and J. L. Volakis, "Embroidered conductive fibers on polymer composite for conformal antennas," *IEEE Trans. Antennas Propag.*, vol. 60, no. 9, pp. 4141–4147, Sep. 2012.

[5] T. Acti *et al.*, "Embroidered wire dipole antennas using novel copper yarns," *IEEE Antennas Wireless Propag. Lett.*, vol. 14, pp. 638–641, Nov. 2014.

[6] Y. Senbokuya and H. Tsunoda, "A study on the circular patch antennas using conductive non-woven fiber fabrics," in *Proc. IEEE Antennas Propag. Soc. Int. Symp.* San Antonio, TX, USA, Jun. 2002, pp. 782–784.

[7] G. Monti, L. Corchia, E. D. Benedetto, and L. Tarricone, "Wearable logo-antenna for GPS–GSM-based tracking systems," *IET Microw., Antennas Propag.*, vol. 10, no. 12, pp. 1332–1338, Sep. 2016.

[8] R. K. Shawl, B. R. Longj, D. H. Werner, and A. Gavrin, "The characterization of conductive textile materials intended for radio frequency applications," *IEEE Antennas Propag. Mag.*, vol. 49, no. 3, pp. 28–40, Jun. 2007.

[9] X. Lin, B.-C. Seet, and F. Joseph, "Fabric antenna with body temperature sensing for BAN applications over 5G wireless systems," in *Proc. 9th Int. Conf. Sens. Technol. (ICST)*, Auckland, New Zealand, Dec. 2015, pp. 8–10.

[10] R. Yahya, M. R. Kamarudin, N. Seman, and H. U. Iddi, "Eye shaped fabric antenna for UWB application," in *Proc. IEEE Antennas Propag. Soc. Int. Symp. (APSURSI)*, Orlando, FL, USA, Jul. 2013, pp. 7–13.

[11] H. A. E. Elobaid, S. K. A. Rahim, M. Himdi, X. Castel, and M. A. Kasgari, "A transparent and flexible polymer-fabric tissue UWB antenna for future wireless networks," *IEEE Antennas Wireless Propag. Lett.*, vol. 16, pp. 1333–1336, Dec. 2016.

[12] W. G. Whittow *et al.*, "Inkjet-printed microstrip patch antennas realized on textile for wearable applications," *IEEE Antennas Wireless Propag. Lett.*, vol. 13, pp. 71–74, Jan. 2014.

[13] A. Chauraya *et al.*, "Inkjet printed dipole antennas on textiles for wearable communications," *IET Microw., Antennas Propag.*, vol. 7, no. 9, pp. 760–767, Jun. 2013.

[14] M. L. Scarpello, I. Kazani, C. Hertleer, H. Rogier, and D. V. Ginste, "Stability and efficiency of screen-printed wearable and washable antennas," *IEEE Antennas Wireless Propag. Lett.*, vol. 11, pp. 838–841, Jul. 2012.

[15] M. Akbari, L. Sydänheimo, Y. Rahmat-Sami, J. Virkki, and L. Ukkonen, "Implementation and performance evaluation of graphene-based passive UHF RFID textile tags," in *Proc. URSI Int. Symp. Electromagn. Theory (EMTS)*, Espoo, Finland, Aug. 2016, pp. 14–18.

[16] L. Alonso-Gonz, S. Ver-Hoeye, M. Fernández-García, Y. Álvarez-López, C. Vázquez-AntuÃśa, and F. L.-H. Andrés, "Fully textile-integrated microstrip-fed slot antenna for dedicated short-range communications," *IEEE Trans. Antennas Propag.*, vol. 66, no. 5, pp. 2262–2270, May 2018.

[17] L. Alonso-Gonzalez, S. Ver-Hoeye, M. Fernandez-Garcia, and F. L. H. Andres, "Three-dimensional fully interlaced woven microstrip-fed substrate integrated waveguide," *Prog. Electromagn. Res.*, vol. 163, pp. 25–38, Oct. 2018.

[18] L. Alonso-Gonzalez, S. Ver-Hoeye, M. Fernandez-Garcia, and F. L. H. Andres, "Layer-to-layer angle interlock 3D woven bandstop frequency selective surface," *Prog. Electromagn. Res.*, vol. 162, pp. 81–94, Jan. 2018.

[19] R. Moro, S. Agneessens, H. Rogier, A. Dierck, and M. Bozzi, "Textile microwave components in substrate integrated waveguide technology," *IEEE Trans. Microw. Theory Techn.*, vol. 63, no. 2, pp. 422–432, Feb. 2015.

[20] R. Moro, S. Agneessens, H. Rogier, and M. Bozzi, "Circularly-polarised cavity-backed wearable antenna in SIW technology," *IET Microw. Antennas Propag.*, vol. 12, no. 1, pp. 127–131, Oct. 2018.

[21] Y. Hong, J. Tak, and J. Choi, "An all-textile SIW cavity-backed circular ring-slot antenna for WBAN applications," *IEEE Antennas Wireless Propag. Lett.*, vol. 15, pp. 1995–1999, Apr. 2016.

[22] S. Yan, P. J. Soh, and G. A. E. Vandenbosch, "Dual-band textile MIMO antenna based on substrate-integrated waveguide (SIW) technology," *IEEE Trans. Antennas Propag.*, vol. 63, no. 11, pp. 4640–4647, Nov. 2015.

[23] M. E. Lajevardi and M. Kamyab, "Ultraminiaturized metamaterial-inspired SIW textile antenna for off-body applications," *IEEE Antennas Wireless Propag. Lett.*, vol. 16, pp. 3155–3158, Oct. 2017.

[24] S. Agneessens, "Coupled eighth-mode substrate integrated waveguide antenna: Small and wideband with high-body antenna isolation," *IEEE Access*, vol. 6, pp. 1595–1602, 2018.

[25] O. Caytan *et al.*, "Half-mode substrate-integrated-waveguide cavity-backed slot antenna on cork substrate," *IEEE Antennas Wireless Propag. Lett.*, vol. 15, pp. 162–165, May 2015.

[26] S. Lemey, F. Declercq, and H. Rogier, "Dual-band substrate integrated waveguide textile antenna with integrated solar harvester," *IEEE Antennas Wireless Propag. Lett.*, vol. 13, pp. 269–272, Jan. 2014.

[27] L. Alonso-González, S. Ver-Hoeye, C. Vázquez-Antuña, M. Fernández-García, and F. L.-H. Andrés, "On the techniques to develop millimeter-wave textile integrated waveguides using rigid warp threads," *IEEE Trans. Microw. Theory Techn.*, vol. 66, no. 2, pp. 751–761, Feb. 2018.

[28] R. Salvado, C. Loss, R. Gonçalves, and P. Pinho, "Textile materials for the design of wearable antennas: A survey," *Sensors*, vol. 12, no. 11, pp. 15841–15857, 2012.

[29] J. Lesnikowski, "Dielectric permittivity measurement methods of textile substrate of textile transmission lines," *Przeglad Elektrotechniczny*, vol. 88, pp. 148–151, Feb. 2012.

[30] K. S. Cole, "Dispersion and absorption in dielectrics I. alternating current characteristics," *J. Chem. Phys.*, vol. 9, no. 4, p. 341, 1941.

[31] C. Gabriel and S. Gabriel. *Compilation of The Dielectric Properties of Body Tissues at RF and Microwave Frequencies*. Accessed: Dec. 10, 2018. [Online]. Available: https://apps.dtic.mil/dtic/tr/fulltext/u2/a305826.pdf

[32] C. Gabriel, S. Gabriel, and E. Corthout, "The dielectric properties of biological tissues: I. Literature survey," *Phys. Med. Biol*, vol. 41, no. 11, pp. 2231–2249, 1996.
[33] S. Gabriel, R. W. Lau, and C. Gabriel, "The dielectric properties of biological tissues: II. Measurements in the frequency range 10 Hz to 20 GHz," *Phys. Med. Biol.*, vol. 41, no. 11, pp. 2251–2269, 1996.
[34] S. Gabriel, R. W. Lau, and C. Gabriel, "The dielectric properties of biological tissues: III. Parametric models for the dielectric spectrum of tissues," *Phys. Med. Biol.*, vol. 41, no. 11, pp. 2271–2293, 1996.
[35] Narda. *Standard Gain Horns, Datasheet*. Accessed: Jun. 20, 2018. [Online]. Available: https://nardamiteq.com/docs/WAVEGUIDEHORNANTENNAS_STANDARD_GAIN_HORNS_2.60_TO_40_GHZ.PDF
[36] Y. Alvarez and F. Las-Heras, "ANCAN: An integrated software tool for the analysis and characterization of antenna arrays," *IEEE Antennas Propag. Mag.*, vol. 49, no. 6, pp. 156–164, Dec. 2007.
[37] Y. Alvarez and F. Las-Heras, "Software tool for antenna array simulation as educational support in telecommunication engineering," *IEEE Antennas Propag. Soc. Int. Symp.*, Albuquerque, NM, USA, Jul. 2006, pp. 9–14.
[38] *IEEE Standard Test Procedures For Antennas*, IEEE Standard 149, 1979.

LETICIA ALONSO-GONZÁLEZ (S'14–M'18) received the M.Sc. degree in systems and control engineering from the National University of Distance Learning (UNED) and the Universidad Complutense de Madrid, Spain, in 2018, and the M.Sc. degree in telecommunications engineering and the Ph.D. degree from the University of Oviedo, Gijón, Spain, in 2014 and 2018, respectively.

Since 2014, she has been a Researcher with the Signal Theory and Communications Group, University of Oviedo. She was a Visiting Scholar with the George Green Institute for Electromagnetics Research, The University of Nottingham, U.K., in 2017. Her main research interests include the design, simulation, and manufacturing techniques to develop micro-wave and millimeter-wave passive circuits and antennas fully integrated in textile technology.

SAMUEL VER-HOEYE (M'05) received the M.Sc. degree in electronic engineering from the University of Gent, Gent, Belgium, in 1999, and the Ph.D. degree from the University of Cantabria, Santander, Spain, in 2002.

He is currently an Associate Professor with the Department of Electrical and Electronic Engineering, University of Oviedo, Gijón, Spain. His main research interests include the design and analysis of nonlinear oscillator-based circuits, millimeter-wave and terahertz antennas, circuits and systems, grapheme-based components, and textile-integrated circuits and antennas.

MIGUEL FERNÁNDEZ-GARCÍA received the M.Sc. degree in telecommunication engineering, the M.Sc. degree in information technology and mobile communications, and the Ph.D. degree from the University of Oviedo, Gijón, Spain, in 2006, 2010, and 2010, respectively.

From 2006 to 2008, he was a Research Fellow with the Signal Theory and Communications Group, University of Oviedo, where he has been an Associate Professor, since 2008. His current research interests include nonlinear analysis and optimization techniques for the design of oscillator-based circuits, active antennas and frequency multipliers and mixers at the microwave, millimeter-/submillimeter-wave, and terahertz frequency bands.

CARLOS VÁZQUEZ-ANTUÑA received the M.Sc. degree in telecommunication engineering, the M.Sc. degree in information technology and mobile communications, and the Ph.D. degree from the University of Oviedo, Gijón, Spain, in 2007, 2008, and 2013, respectively.

From 2007 to 2012, he was a Graduate Research Assistant with the Signal Theory and Communications Group, University of Oviedo, where he has been a Research Fellow, since 2012. His research interests include nonlinear analysis and optimization techniques for the design of multifunctional oscillator-based circuits, active antennas, and passive components, such as frequency multipliers and harmonic mixers, at microwave, millimeter-/submillimeter-wave, and terahertz frequencies.

FERNANDO LAS-HERAS ANDRÉS (M'86–SM'08) received the M.S. and Ph.D. degrees in telecommunication engineering from the Technical University of Madrid (UPM), Madrid, Spain, in 1987 and 1990, respectively.

He was a National Graduate Research Fellow and an Associate Professor with the Department of Signal, Systems and Radiocom, UPM, from 1988 to 1990 and from 1991 to 2000, respectively. He was the Vice-Dean of Telecommunication Engineering, Technical School of Engineering, Gijón, Spain, from 2004 to 2008. He was a Visiting Researcher with Syracuse University, New York, NY, USA, and a Visiting Lecturer with the National University of Engineering, Lima, Peru, and the École Supérieure d'Ingénieurs en Génie Électrique, Rouen, France. He has been the Head of the Signal Theory and Communications Research Group, Department of Electrical Engineering, University of Oviedo, Gijón, since 2001, and has been a Full Professor, since 2003. He has authored over 450 technical journal and conference papers in the areas of electromagnetic radiation, propagation and scattering theory and applications, as well as inverse problems.

Dr. Andrés was a member of the Science, Technology and Innovation Council of Asturias, Spain, in 2010, and the Board of Directors of the IEEE Spain Section, from 2012 to 2015. He was currently a member of the IEEE Microwaves and Antennas Propagation Chapter (AP03/MTT17) Board, from 2016 to 2018. He was the Telefónica Chair of the RF Technologies, ICTs Applied to Environment and Climate Change, and the ICTs and Smartcities, from 2005 to 2015.